Materials Research Proceedings 28 (2023) 119-127 https://doi.org/10.21741/9781644902479-14

Influence of process parameters and head orientation on bead geometry for coaxial wire laser additive manufacturing

ROCH Clément[1,a *], TOURNIER Christophe[1,b] and LAVERNHE Sylvain[1,c]

[1] Université Paris-Saclay, ENS Paris-Saclay, LURPA, 91190, Gif-sur-Yvette, France

[a]clement.roch@ens-paris-saclay.fr, [b]christophe.tournier@ens-paris-saclay.fr, [c]sylvain.lavernhe@ens-paris-saclay.fr

Keywords: Additive Manufacturing, Laser Wire, Bead Geometry

Abstract. Among Directed Energy Deposition (DED) processes for metallic materials, Wire Laser Additive Manufacturing (WLAM), distinguishes itself by the use of a laser beam to melt a metallic wire and produce beads. Successive depositions of overlapping beads generate volumes to obtain parts. Thus, controlling bead geometries is essential for the additive manufacturing process. Several research works have studied these geometries and the influence of the main manufacturing parameters on their dimensions, but few investigated the effect of feeding direction or wire angle. Moreover, all studies on wire angle were carried out with lateral feeding and a constant laser orientation. This paper focuses on the influence of the deposition head orientation for a coaxial wire feed with 3 laser beams on bead geometries. An experimental campaign is conducted with different orientations relatively to a horizontal substrate and the external profiles are measured using optical instruments in order to extract the average profiles and characteristic dimensions. Results indicate an influence of the head rotation around its axis and lateral tilt on the height, width, and asymmetry of the beads.

Introduction

Metal additive manufacturing represents a major challenge for the development of new production strategies. Several processes are already in use, with either powder or wire as feedstock material. The use of wire results in simpler installations by reducing the constraints linked to powder handling, while producing solid parts with large volumes, as observed in Wire Arc Additive Manufacturing (WAAM). Wire Laser Additive Manufacturing (WLAM) is also based on a metallic wire, but with a laser beam as energy supply. Several configurations can be found in this category, depending on different technological choices or additional elements. For example, hot-wire limits the laser power required for manufacturing [1]. Differences are also possible in terms of material and power input, as the wire can be supplied along a different axis as the laser beam or along the same one, resulting in a coaxial configuration. This technology can be achieved by the use of multiple laser beams [2] or a ring beam [3].

Because of the wide variety of experimental devices and possible use cases, each installation requires the set-up of manufacturing recipes, often in an empirical manner by conducting several experiments. The usual approach consists in manufacturing single beads to define the initial process parameters, then in the study of overlapping beads to obtain surfaces, and finally in the study of layers, for single-bead walls or massive parts. Two profiles can be identified to describe single bead geometry: the external profile, also called reinforcement, and the internal profile, called penetration (Fig. 1). Rather than describing the complete geometries, specific dimensions are often used to characterize beads, as seen in figure 1 with width W, height H, contact angle θ_c and penetration P. Other typical dimensions not shown in the figure are the cross-section area A, which is considered as the additional area relatively to the initial part, and the dilution ratio, defined by the ratio between the area of the bead penetrating the substrate and the total area.

The existing literature proposes several models to describe the reinforcement profiles, including elliptical [4,5], sinusoidal [6] or polynomial models of degree 2 [7,8] or 4 [9]. A comparative study by Ding et al [10] highlights that most of these models present a satisfactory representation of the beads, while Xiong et al [11] establish that the optimal model is linked to the ratio between wire feed speed and travel speed. Most studies focus on relations between bead dimensions and the main process parameters: laser power, wire feed speed and travel speed, showing that width and height can vary independently. Abioye et al [12] and Medrano-Tellez [13] establish that the link between power and wire feed speed is essential to guarantee stability, with two main process defects: dripping when power is too high compared to wire speed and stubbing when it is too low.

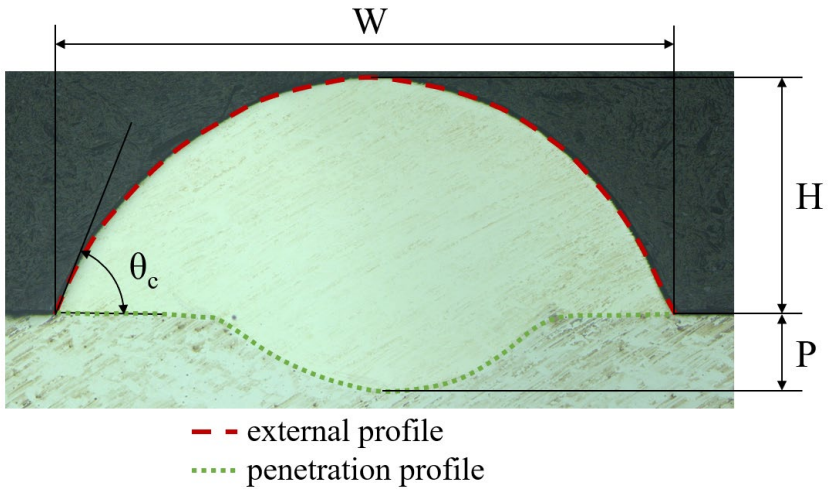

Fig. 1. Cross section of a bead with its dimensions.

One study focuses on feeding direction and found that it influences the appearance of the beads, with front feeding resulting in smoother beads [14]. For lateral configurations, where both laser beam and wire have different axes, the angle between wire and substrate also influences the produced geometries. However, the deposition head considered in this study uses three laser beams distributed around the wire to obtain a coaxial configuration. No articles investigating the influence of orientation and inclination on bead geometry for coaxial heads were found in the available literature. Most papers for coaxial technologies focus exclusively on wire feed speed, travel speed and laser power, with an occasional mention of the distance between the beams intersection point and the workpiece [15]. However, head orientation relatively to the travel direction can vary during manufacturing. In addition, variations in head tilt relatively to the substrate can be used to gain collision-free access to specific areas of the workpiece, or to manage gravity.

Therefore this study focuses on whether the tilt and orientation angles of a 3-beam coaxial head to the substrate have an effect on produced external bead geometries. This paper presents the experimental setup and process conditions before describing the method used to identify the effect of both head tilt and rotation. The obtained results are then presented and discussed before concluding.

Experimental Setup

The additive manufacturing cell (Fig. 2) is based on laser-wire technology, implemented by a Coaxworks head carried on a ABB IRB4600 robot and using an Ytterbium fibre laser power source with a maximum power of 4 kW. The feedstock is a 1.2 mm diameter IN718 wire and the parts are produced on S235 JR steel substrates which are 80mm long, 40mm wide and 10mm thick. A Xiris weld monitoring camera is attached to the head, enabling process monitoring. In addition,

the head's optics are protected by a flow of compressed air to expel smoke and spatters, and the weld pool is protected from oxidation by a flow of Argon at a pressure of 2 bars.

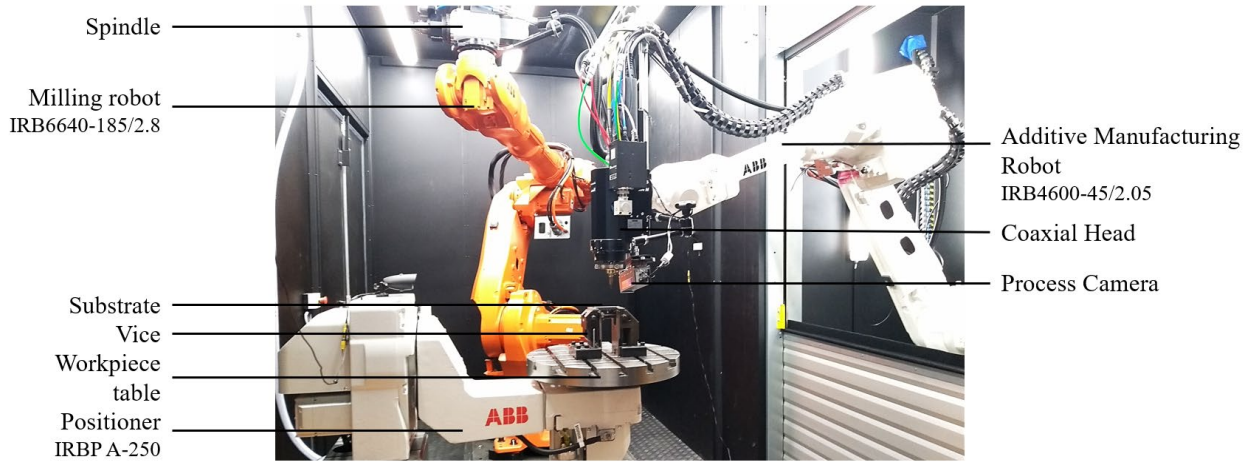

Fig. 2. Overview of the WLAM setup.

The head divides the initial beam into three laser beams, equally placed around the vertical axis of the head (z-axis) at 90, 150 and 30° angles to the x-axis respectively for beams 1, 2 and 3, and with an angle of 17.5° to z. In standard production configuration, the head is oriented so that its z-axis follows gravity.

Initial tests established a process window depending on three usual parameters (power, wire feed speed and travel speed) regarding both stubbing and dripping defects. In addition, two additional phenomena were observed. At low laser power and low wire speed, lack of fusion appears (Fig. 3a), where the energy is sufficient to melt the wire, but not the substrate, resulting in a bead without adherence. This phenomenon was already observed by Medrano Tellez [13], who characterizes it by a head speed too high for the power. In contrast, with low travel speed and high wire feed speed while keeping sufficient laser power to melt it, a wider and higher melt pool than other beads is obtained. Its behaviour is close to that of a liquid (Fig. 3b), similar to what can be observed in WAAM.

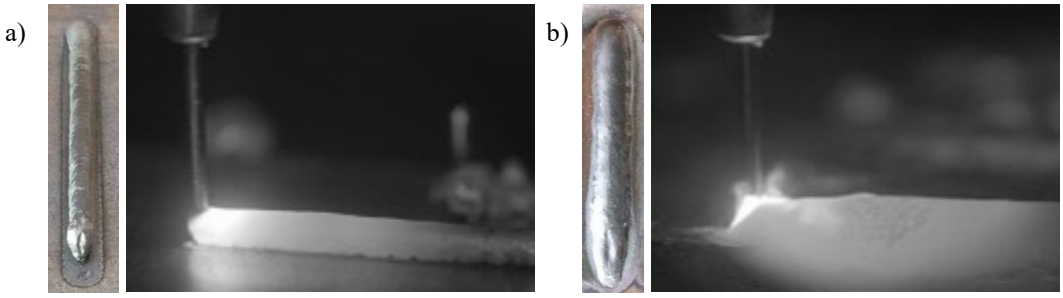

Fig. 3. Beads and process views for two defects: lack of fusion on the left and liquid behaviour on the right.

Method

According to the process window, an operating point with a travel speed of 1 m/min, a wire speed of 2 m/min and a power of 2.2 kW is used for all experiments. These parameters were determined with a working distance of 2 mm, which means that the intersection point of the three laser beams is 2 mm below the substrate surface. The dotted red segments on figure 4 stand for the axes of the

three laser beams, the continuous red segment for the head axis, and the black outline for the laser spot boundaries.

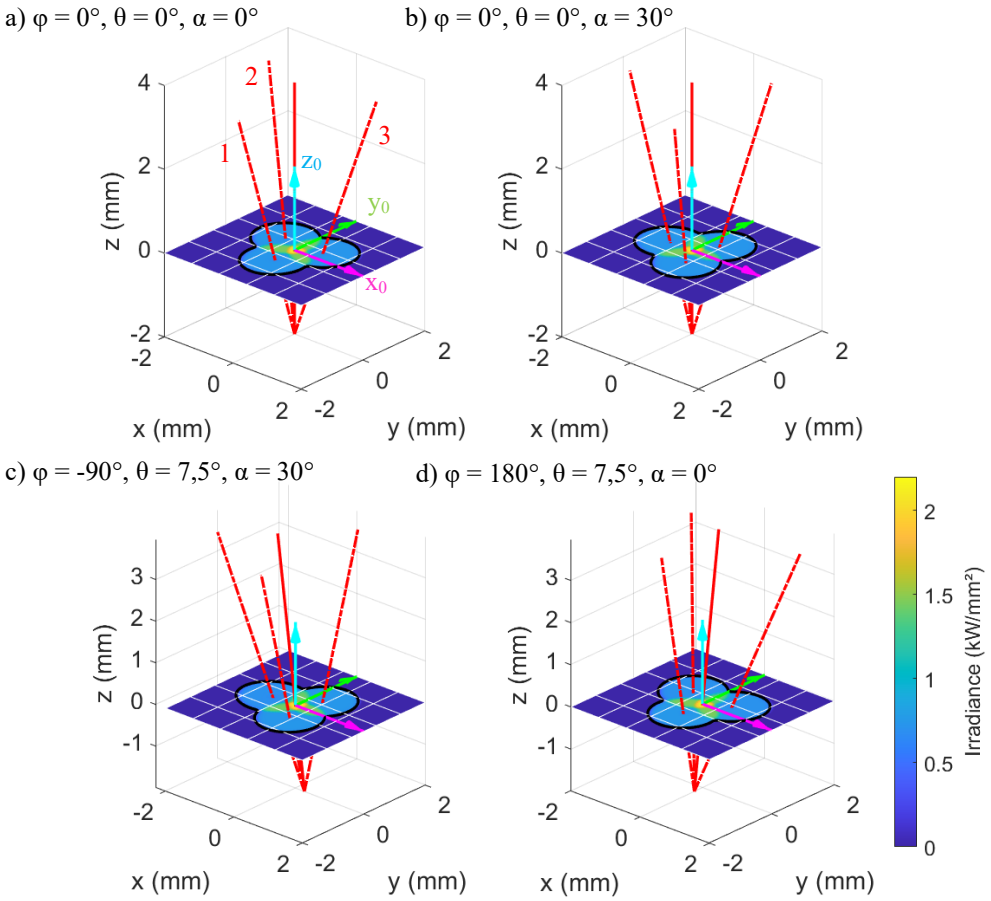

Fig. 4. Power density and laser spot limit for different head orientations.

During manufacturing the substrates remain fixed and the head travels along the x_0 axis of the substrate in the positive direction, with different orientations. To describe the head orientation, an intrinsic Euler formalism is used, corresponding to a rotation of angle φ (precession) about z_0, corresponding to the tilting direction, followed by a rotation of angle θ, called tilt, about x' and finally a rotation of angle ψ about z''. The angle $\alpha = \psi + \varphi$ will be used and referred to as head rotation, as it approximates the total rotation of the head around its axis when θ is small (0.2° deviation for θ = 7.5°). The limits of these angles are fixed by technological constraints (cable management and laser safety), with α constrained in the interval [-70°;70°] and θ inferior to 8°. For the experiments θ varies on two levels between 0 and 7.5°, φ on 8 levels between 180 and 135°, and α on 5 levels between -60 and 60°. Only the value φ = 0° is considered for θ = 0°. Therefore 45 tests were carried out, with four 60 mm beads deposited on each substrate, spaced 8 mm apart with a waiting time of around 1 minute to reduce the possible effects of thermal accumulation. Preliminary tests established that geometries of beads produced under these conditions are independent of manufacturing order. The produced parts were measured using an optical 3D measurement system over an area of 3.6 mm by 3.6 mm in the bead centre. The deposition direction x_0 was identified before subdividing the y_0 axis into 1000 intervals between -2 and 2 mm, resulting in a local height distribution for each value of y, corresponding to the variations in height inside the measurement window. The mean value and the standard deviation σ of the z values according to y were determined, leading to a statistical bead profile over the entire

measured area. Under the assumption of a Gaussian distribution of the values, a 95% confidence interval can be considered as ±1.96 σ. Using this mean profile, the parameters H, W and A were determined with their confidence intervals. A new value A_r is added, which represents the ratio between the area on the right of the bead (corresponding to positive values of y) to the total area, with the middle of the base serving as centre. This value is only determined for the mean profile and expresses if the bead is tilted to one side, serving as an indicator for asymmetry.

Results and Discussion

Among the 5 beads produced with θ = 0° and varying α, the angles α = -60° and α = -30° present stubbing, contrarily to the other beads which have a smooth appearance (Fig. 5). For α = -60°, the measurement area is not located in the centre but close to the start when stubbing is not as apparent. The dimensions as functions of the angle α are displayed on Fig. 6. The confidence interval for α = -30° is much larger than for the other values, while it does not appear for α = -60° after the measurement zone shift.

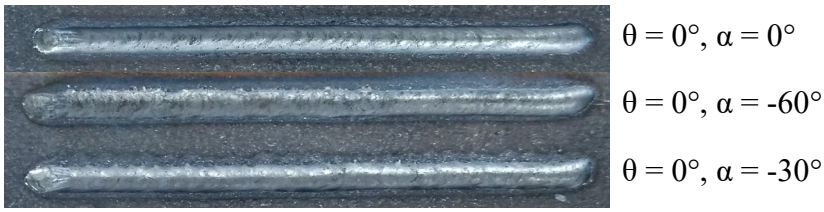

Fig. 5. Beads with or without stubbing (welding direction from right to left).

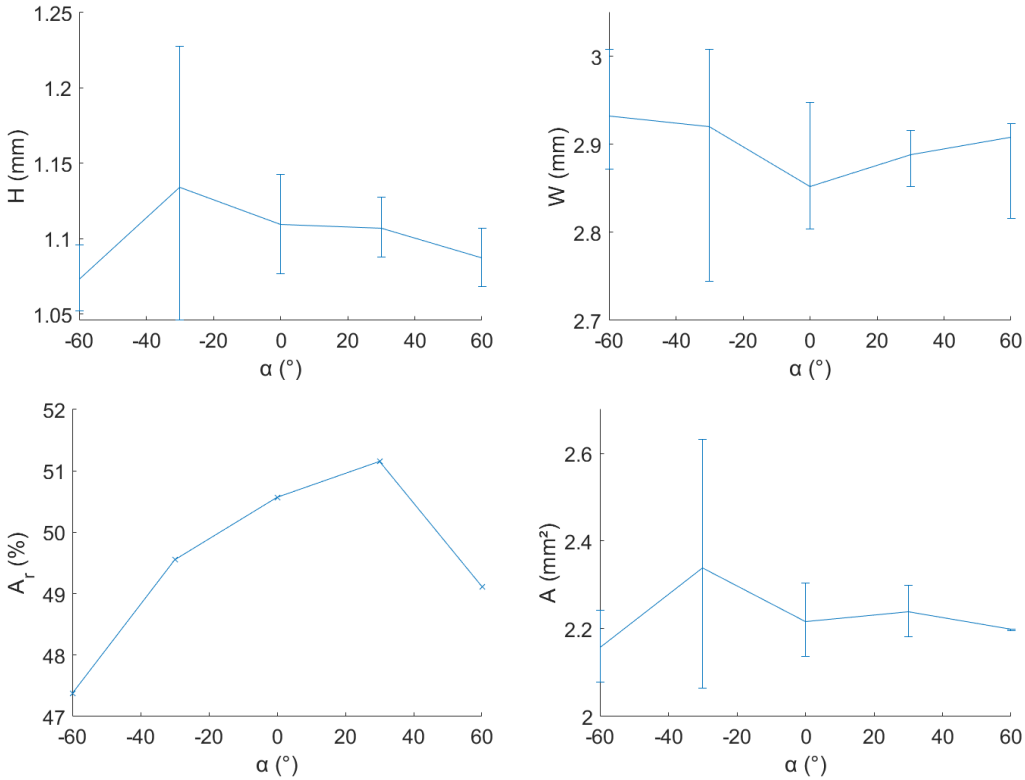

Fig. 6. Variations in bead dimensions for different head rotations.

These results do not show a significant evolution of the dimensions depending of the head rotation, except for A_r. This variation limited to around 4% of bead area indicates that the rotation without head tilt may introduce a slight asymmetry in bead profiles. It is notable that the configuration corresponding to an almost even ratio between left and right is achieved with α = -

Materials Research Proceedings 28 (2023) 119-127 https://doi.org/10.21741/9781644902479-14

30°, which places the beam number 3 on the front and the other two on the back, resulting in a symmetrical distribution on both sides of the melt pool (Fig. 4). Moreover, more matter is displaced to the right when beam 3 is placed on the side where y is positive, and more on the left when on the y negative side.

Some configurations with θ = 7.5° lead to dripping at the start of the bead, where a drop of material remains on the wire before being deposited, leading to a shifted start of the bead (Fig. 7). The rest of these beads is stable, which would rather indicate a defect in the starting parameters, particularly the duration between wire positioning and laser start. The variations in dimensions as a function of φ for different values of α are plotted in figure 8, and the dripping conditions do not lead to a wider interval, except for φ = -135°, α = -30°.

Fig. 7. Beads with dripping at the start.

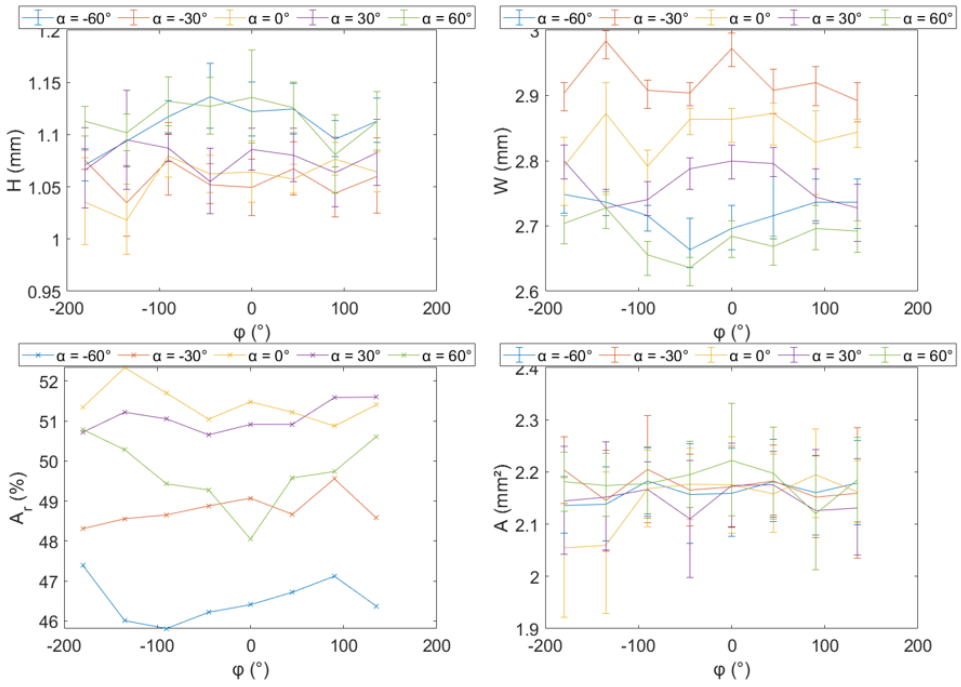

Fig. 8. Variations in bead dimensions for θ = 7.5°.

No significant variations in bead area can be observed, as the differences between mean values are inferior to the confidence intervals. This was expected as the ratio of wire feed speed to travel speed remains constant. Changes can be observed for the width and height, but they remain small (around 10%) and seem to be more related to head rotation than to the tilting direction. To help in the geometry comparison, 5 profiles are selected and displayed on Fig. 9.

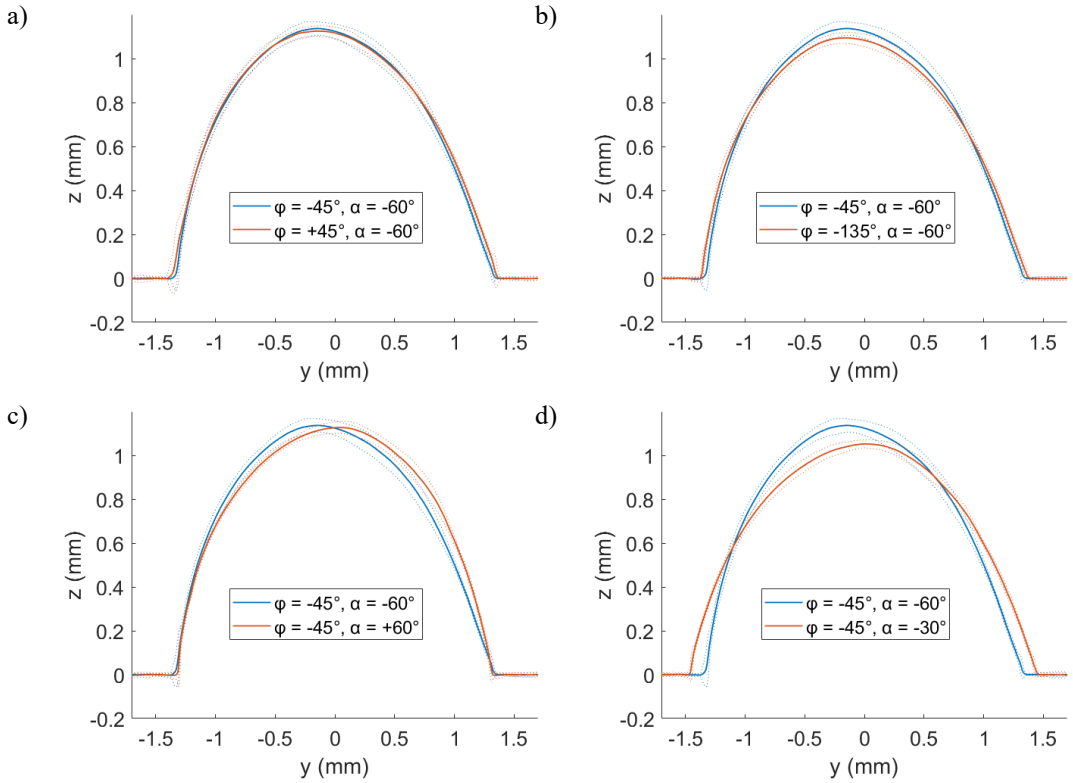

Fig. 9. Comparison of selected bead profiles for θ = 7.5°.

The width seems to depend little on the tilting direction, but more on the head rotation when the head is tilted (Fig. 8), whereas it does not seem to vary without tilt. Indeed, the widths for α = 60° are always smaller than those obtained for α = 0°, in turn smaller than for α = -30°. Fig. 9d compares beads and illustrates the width variation. The maximum width is then obtained for α = -30°, which corresponds to the only configuration tested where one laser beam is at the front of the wire and two beams are at the back (Fig. 10). The effects of head rotation on the ratio between area on the right and total area are observed again, and Fig. 9c shows the asymmetry in the full profile between two orientations.

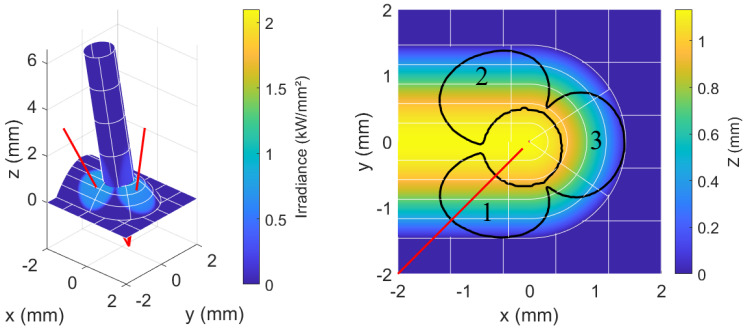

Fig. 10. Laser spot on a nominal bead model with θ = 7.5°, φ = -45° and α = -30°, 3D view on the left and top view on the right.

In contrast to the two previous quantities, bead height depends on the tilting direction. Indeed, variations due to the angle φ are greater than those observed by varying the angle α, but only for α = 60 or -60°. The height of the beads therefore depends on both tilting direction and head rotation. To ease the analysis, the head axis and laser spots are plotted in Fig. 11 for all the configurations of Fig. 9.

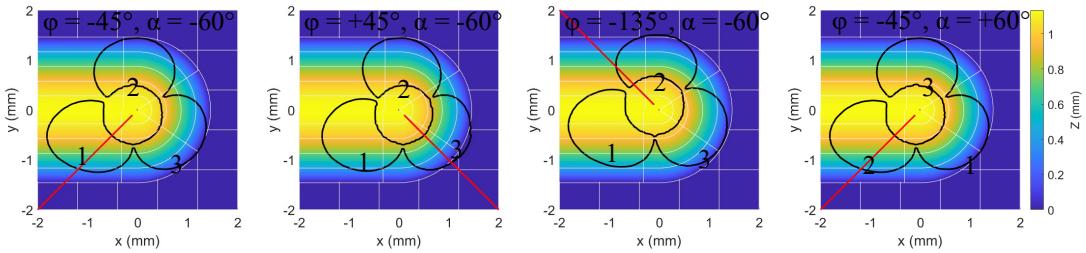

Fig. 11. Comparison of the different configuration of Fig. 9.

For the following discussion two terms are introduced: the front/back tilt to describe the angle around the y axis, and the lateral tilt to describe the angle around x. Thus, between φ = 45 and +45° lateral tilt does not vary, while the head is tilted either towards the front (φ = +45°) or the back (φ = 45°) of the melt pool. Fig. 9a shows that this variation from front to back tilting does not affect bead profile significantly. Fig. 9b highlights that change in lateral tilt leads to change in height without affecting width. Maximum height is obtained by tilting the head to the left side, where two beams are located. Indeed, as seen in figure 11, both α = 60 and -60° correspond to configurations where one laser is aligned with the y axis and on the right side (y positive). However, the configuration α = 0° also corresponds to a beam aligned with the y axis, but no link between α and H is observed for this value. When α = 0°, beam number 1 is aligned with y and located to the left of the profile, while for α = 60° it is beam 3 on the right side and beam 2 on the right side for α = -60°. The observed variations may also be influenced by defects in the power distribution between the beams, or defects in wire positioning. Further studies would allow to quantify their effects on the presented results.

Summary

In this paper the influence of orientation parameters on single beads external geometries was investigated. The beads were measured to extract mean profiles with their associated confidence intervals, allowing to obtain dimensions for the different tested angles. Results showed that head rotation mainly influences the width and asymmetry of the beads, with symmetrical and wide beads obtained when one beam is placed at the front and two beams at the back. For configurations with one beam on one side of the melt pool and the other two on the opposite side, the height of the bead depends on the lateral tilt of the head. No influence of front or back tilting was observed in this study.

The measured variations for a tilt angle up to 7.5° are around 10% of nominal values. A higher tilt angle could amplify these effects but achieving it on this setup would require using the 2-axis positioner, changing gravity direction relatively to the part. This study focused on external geometries without studying the penetration. However, a change in power density can lead to variations in bead-substrate interactions. Further analysis of dilution and penetration are part of the perspectives of this work.

Acknowledgement

We thank Adel Abbas for his help in measuring the manufactured beads.

References

[1] Z. Nie, G. Wang, J.D. McGuffin-Cawley, B. Narayanan, S. Zhang, D. Schwam, M. Kottman, Y. Rong, Experimental study and modeling of H13 steel deposition using laser hot-wire additive manufacturing, J. Mater. Process. Technol. 235 (2016) 171-186. https://doi.org/10.1016/j.jmatprotec.2016.04.006

[2] F. Du, J. Zhu, X. Ding, Q. Zhang, H. Ma, J. Yang, H. Cao, Z. Ling, G. Wang, X. Duan, S. Fan, Dimensional characteristics of Ti-6Al-4V thin-walled parts prepared by wire-based multi-laser

additive manufacturing in vacuum, Rapid Prototyp. J. 25 (2019) 849-856. https://doi.org/10.1108/RPJ-08-2018-0207
[3] A. Ayed, G. Bras, H. Bernard, P. Michaud, Y. Balcaen, J. Alexis, Study of Arc-wire and Laser-wire processes for the realization of Ti-6Al-4V alloy parts, MATEC Web of Conferences 321 2020. https://doi.org/10.1051/matecconf/202032103002
[4] W. Aiyiti, W. Zhao, B. Lu, Y. Tang, Investigation of the overlapping parameters of MPAW-based rapid prototyping, Rapid Prototyp. J. 12 (2006) 165-172. https://doi.org/10.1108/13552540610670744
[5] A. Sharma, N. Arora, B. Mishra, Mathematical Model of Bead Profile in High Deposition Welds, J. Mater. Process. Technol. 220 (2015) 65-75. https://doi.org/10.1016/j.jmatprotec.2015.01.009
[6] Y. Cao, S. Zhu, X. Liang, W. Wang, Overlapping model of beads and curve fitting of bead section for rapid manufacturing by robotic MAG welding process, Robot. Comput.-Integr. Manuf. 27 (2011) 641-645. https://doi.org/10.1016/j.rcim.2010.11.002
[7] G.H. Kim, S.I. Kang, S.B. Lee, Study on the estimate of weld bead shape and the compensation of welding parameters by considering weld defects in horizontal fillet welding, International Conference on Knowledge-Based Intelligent Electronic Systems, 2000, pp. 212-216. doi:10.1109/KES.1999.820157
[8] S. Suryakumar, K.P. Karunakaran, A. Bernard, U. Chandrasekhar, R. Nadella, D. Sharma, Weld bead modeling and process optimization in Hybrid Layered Manufacturing, Computer-Aided Des. 43 (2011) 331-344. https://doi.org/10.1016/j.cad.2011.01.006
[9] M. Kumar, S.S. Kumar, A. Sharma, Bi-polynomial fourth-order weld bead model for improved material utilization and accuracy in wire-arc additive manufacturing: A case of transverse twin-wire welding, Adv. Industr. Manuf. Eng. 2 (2021) 100049. https://doi.org/10.1016/j.aime.2021.100049
[10] D. Ding, Z. Pan, D. Cuiuri, H. Li, A multi-bead overlapping model for robotic wire and arc additive manufacturing (WAAM), Robot. Comput.-Integr. Manuf. 31 (2015) 101-110. https://doi.org/10.1016/j.rcim.2014.08.008
[11] J. Xiong, G. Zhang, H. Gao, L. Wu, Modeling of bead section profile and overlapping beads with experimental validation for robotic GMAW-based rapid manufacturing, Robot. Comput.-Integr. Manuf. 29 (2013) 417-423. https://doi.org/10.1016/j.rcim.2012.09.011
[12] T.E. Abioye, J. Folkes, A.T. Clare, A parametric study of Inconel 625 wire laser deposition, J. Mater. Process. Technol. 213 (2013) 2145-2151. https://doi.org/10.1016/j.jmatprotec.2013.06.007
[13] A.G. Medrano-Tellez, Fiber laser metal deposition with wire: parameters study and temperature control, PhD Thesis, University of Nottingham, 2010.
[14] S.H. Mok, G. Bi, J. Folkes, I. Pashby, Deposition of Ti-6Al-4V using a high power diode laser and wire, Part I: Investigation on the process characteristics, Surf. Coat. Technol. 202 (2008) 3933-3939. https://doi.org/10.1016/j.surfcoat.2008.02.008
[15] S. Ocylok, M. Leichnitza, S. Thieme, S. Nowotny, Investigations on laser metal deposition of stainless steel 316Lwith coaxial wire feeding, 9th International Conference on Photonic Technologies (LANE 2016), 2016.